RSC Advances

PAPER

View Article Online
View Journal | View Issue

Cite this: RSC Adv., 2014, 4, 39576

Influence of in-plane Stone–Thrower–Wales defects and edge functionalisation on the adsorption of CO_2 and H_2O on graphene†

Lalitha Murugan,[ab] Senthilkumar Lakshmipathi*[ab] and Suresh K. Bhatia*[a]

There is now increasing recognition of the potential of graphene membranes for gas separation, with the application to CO_2 capture being one of specific interest; however, the co-adsorption of H_2O which saturates flue-gas remains a major impediment. Towards enhancing hydrophobic characteristics of graphene while increasing specificity to CO_2, we investigate here the adsorption characteristics of CO_2 and H_2O on four different kinds of graphene sheet – namely, hydrogen-terminated and fluorine-terminated pristine sheets, and the corresponding Stone–Thrower–Wales (STW) defect-incorporated sheets using density functional theory methods. Our results reveal that fluorine termination enhances hydrophobicity and favours the adsorption of CO_2, while reducing that of H_2O, in comparison to hydrogen termination. On the other hand, H_2O adsorption affinity is increased on introducing the Stone–Thrower–Wales defect in both H-terminated and F-terminated sheets, while for CO_2 the affinity change is more marginal, evidenced from the change in height of the adsorbed molecule above the surface, and of the adsorption energy. The Henry law constant for H_2O is reduced by 54% on F-termination, for both pristine and defective H-terminated graphene sheets, while for CO_2 it is increased by 12% and reduced by 18% respectively, on F-termination of the two sheets; indicating the pristine F-terminated sheet as the preferred option. From the density of states analysis, the Fermi level shows a 0.7 eV shift towards the valence band for fluorine termination in both pristine and STW sheets, but is not influenced by CO_2 and H_2O adsorption. Fluorine termination is shown to have a significant effect on the valence band, and offers a convenient route for tuning the electronic structure of graphene.

Received 24th June 2014
Accepted 13th August 2014

DOI: 10.1039/c4ra06184e

www.rsc.org/advances

1. Introduction

Graphene is a 2d nanomaterial comprising a monolayer of sp^2 hybridized carbon atoms, that is attracting enormous interest because of its unique electronic, optical, mechanical and surface properties, which have the potential to enable a wide range of applications, besides offering new opportunities in fundamental physics.[1] Among the applications under investigation are those in battery and electrochemical energy storage,[2] electronics and semiconductor devices,[3] biodiagnosis and biomedicine,[4] and membranes for gas separation.[5,6] The critical feature of graphene that influence its performance in these applications is its electronic structure, which governs its conductivity as well as interaction with adsorbed fluids. The inherent electronic structure of graphene can be dramatically modified by the kind of functionalisation used to terminate (*i.e.* passivate) its edge sites,[7] and the presence of in-plane defects, importantly Stone–Thrower–Wales[8,9] (STW) defects. Brenner *et al.*[7] experimentally demonstrate orders of magnitude in enhancement in the density of charge carriers on edge doping, which in turn leads to large increase in conductivity. Such changes in electronic structure will also affect the adsorption affinity of graphene, with the extent depending on the adsorptive in question. For example, drastic changes in the electronic structure of graphene have been theoretically estimated when edge sites are terminated by fluorine,[10] leading to enhancement in hydrophobicity.[11–13] On the other hand high moisture and water transport rates have been observed in a nanoporous graphene membrane having edges terminated by oxygen-containing moieties[14] (although some H-termination was not discounted), suggesting hydrophilicity. Using DFT Santos *et al.*[15] explored the hydrogenation and fluorination at different concentration and sites of corannulene, and showed that the fluorination is energetically more favourable than hydrogenation of corannulene. Such results emphasise the significant effect of the edge-terminating group in graphene on its adsorption properties.

Studies with nanoporous graphene membranes have confirmed the importance of appropriate choice of edge group.

[a]School of Chemical Engineering, The University of Queensland, St. Lucia, QLD 4072, Australia. E-mail: s.bhatia@uq.edu.au

[b]Department of Physics, Bharathiar University, Coimbatore-641046, Tamil Nadu, India. E-mail: lsenthilkumar@buc.edu.in

† Electronic supplementary information (ESI) available. See DOI: 10.1039/c4ra06184e

Extremely high H_2/CO_2 selectivities of the order of 10^8 with high H_2 permeance have been theoretically estimated when the edge sites are passivated by nitrogen, and even higher selectivity for H_2/CH_4 separation estimated with edge sites functionalised by hydrogen.[5] Similarly, fluorine functionalisation of edge groups has been theoretically shown to enhance CO_2 permeation and CO_2/N_2 selectivity in nanoporous graphene,[6] by decreasing the energy barrier for CO_2 while increasing that for N_2. An obvious effect of functionalisation is that of modulating pore size, evident from comparison of MD simulations of permeation through unfunctionalised nanoporous graphene with experimental data;[16] these show large overprediction at small pore size where functionalisation is expected to significantly reduce the accessible aperture size. All of these studies demonstrate the importance of appropriate edge-functionalisation in promoting selectivity; nevertheless, the mechanism by which this is achieved, besides affecting accessible pore size, is an issue requiring further investigation.

Besides nanoporous graphene membranes, appropriate choice of edge-functionalising agent is also relevant to nanoscale membranes comprising stacked graphene layers, a subject of recent attention.[17,18] Unexpected defect-mediated selective permeation in graphene oxide (GO) membranes has been reported, with H_2/CO_2, O_2/N_2 and CO_2/N_2 selectivities exceeding those of state-of-the-art microporous membranes.[17,18] The defects are considered to be structural, governed by the degree of interlocking of the graphene layers.[18] An interesting finding reported by Kim *et al.*,[18] is that while permeances of H_2, N_2 and O_2 decreased on increasing humidity, that of CO_2 increased by a factor of 50, leading to selectivity increase for carbon dioxide. Although the permeability decrease is likely due to the hydrophilic nature of GO and the consequent greater water adsorption at higher humidity, the reason for the large increase for CO_2 is not obvious. Indeed, quite the opposite effect is predicted by Yumura and Yamasaki,[19] whose density functional theory calculations indicate reduction in interlayer spacing in GO, and increase in the barrier for CO_2 migration, as a result of hydration. On the other hand, significant low pressure enhancement of CO_2 adsorption by pre-adsorbed water in carbon nanotubes, due to the effect of CO_2/H_2O interactions, particularly when the water is present as small clusters, has recently been reported by Liu and Bhatia.[20] The possibility therefore exists that adsorbed water is present as small clusters in GO membranes, due to the highly confined and disordered nature of the interlocking spaces, which is supported by the findings of Nguyen and Bhatia[21,22] on the adsorption and dynamics of water in disordered carbons. Nevertheless, regardless of the mechanisms involved, these findings suggest the importance of investigating the effects of edge functionalisation on adsorption on graphene surfaces.

Various kinds of defects, such as vacancies, substitutional impurities, adatoms and topological imperfections are formed during the growth of graphene,[23] and are known to significantly alter its electronic structure and adsorption properties.[24] Gueorguieve *et al.*[25] carried out a first-principle investigation of defects in carbon-phosphide structures (CP_x) and found that tetragon defects are energetically stable in CP_x, and also inhibit buckling in the graphene sheets, which provides fullerene like shape. The Stone–Thrower–Wales[8,9] defect is a typical topological defect in carbons,[26,27] arising from bond rotation and rearrangement of four six-membered rings into two pentagons and two hexagons. Besides being formed during graphene synthesis, such defects can also be introduced by electron irradiation,[28–30] and have been imaged using transmission electron microscopy.[31] While such defects have been theoretically shown to have negligible effect on the hydrophilic or hydrophobic properties of graphene,[32] they appear to improve its adsorption affinity for several other molecules. Thus, Dutta *et al.*[33] report enhancement of the binding strength of CO_2 by defects in graphene, compared to the pristine material. In particular, they find 20–25% increase in binding energy of CO_2 on introduction of the Stone–Thrower–Wales defect. In other work, Zhang *et al.*[24] report significant increase in adsorption energy of CO, NO and NO_2 on defective graphene over its pristine counterpart, with B- or N-doping giving somewhat lower enhancement. Similarly, enhancement of H_2CO binding with and without Al dopant, and of ethanethiol binding, on introduction of the STW defect in graphene is reported by Qin *et al.*,[34,35] based on the density functional theory (DFT) calculations. The STW defect has also been shown to stabilize adsorbed hydroxyl groups on the graphene surface,[36] increasing binding energy and the barrier for recombination to form water. These and other studies[37] suggest that significant sensitivity enhancement in the gas sensing performance of graphene can be achieved on defect introduction.

A separation where the effects of functionalisation and defects is particularly important is that of CO_2 from flue gas, for which graphene has been suggested to have good potential.[38] This separation is relevant to the important area of carbon capture, now the subject of a major world-wide effort due to the significant climate change effects associated with the large emissions of CO_2 arising from human activity. However, while the capture of CO_2 using mesoporous or nanoporous materials is receiving widespread attention,[39–43] a significant concern is that of co-adsorption of water which saturates flue gas. Since water is strongly adsorbed on hydrophilic materials such as zeolites and metal–organic framework materials,[18,20] it has the potential to severely degrade the performance of an adsorbent, and the use of a hydrophobic carbon has been suggested as a preferred option.[39] The emerging nanoporous or stacked graphene membranes with fluorine functionalisation to enhance hydrophobicity would appear to be a potentially promising option. Further, the effect of defect introduction with simultaneous fluorine-termination of edge sites on H_2O and CO_2 adsorption would be particularly interesting, because of the potential to selectively inhibit water adsorption while enhancing interactions with CO_2.

In the present work, we investigate the effect of simultaneous STW defect introduction and fluorine/hydrogen-termination at the edges of the graphene sheet on the adsorption of CO_2 and H_2O using the density functional theory. For comparison, the pristine graphene sheet functionalised with hydrogen and fluorine atoms at edges is also studied. Recent work[16] has shown that surface adsorption has an important influence on

the flux in nanoporous membranes and, except for non-adsorbing gases, the surface flux can be comparable to the direct pore flux. Thus, while we investigate adsorption on the edge-functionalised sheet with STW defects but without introduction of pores, the results are relevant even for separation using nanoporous graphenes. The results from this work provide fundamental insights into the adsorption properties of CO_2 and H_2O on the H and F edge-terminated graphene sheet with STW defect, and the effects of these strategies on the selectivity of CO_2 over H_2O.

2. Computational details

We constructed a rhombic 4 × 4 graphene sheet of side ~9.77 Å, having a total of 48 carbon atoms depicted in Fig. 1. The graphene sheet is functionalised along its edges with 18 hydrogen or fluorine atoms. Further, the Stone–Thrower–Wales defect is incorporated in the center of both hydrogen and fluorine passivated sheets. For convenience, we label the structures as P-Gr/H, P-Gr/F, STW-Gr/H, STW-Gr/F, where P-Gr represents pristine (P) graphene (Gr) and STW-Gr denotes Stone–Thrower–Wales (STW) incorporated graphene (Gr) sheet and /H, /F denotes the edge functionalised by hydrogen and fluorine atoms respectively. For further discussion, pristine sheet refers to the sheet without any defect. Gas molecules such as CO_2 and H_2O are adsorbed on these four kinds of sheets. For the pristine sheet, in total there are three sites of adsorption, shown as top (T), bridge (B) and hollow (H) in Fig. 2. In the case of the adsorption of CO_2, as it is a linear molecule, there are two possible orientations with respect to the graphene sheet; these are the parallel orientation of CO_2 as shown in Fig. 2, and the perpendicular position with the oxygen pointing towards the sheet, as depicted in Fig. 3. When a STW defect is introduced in the sheet, the possible sites of adsorption on the hollow site splits into two as: one on the heptagon ring (H-hept) and the other on the pentagon ring (H-pent) of the defect as shown in Fig. 4a and b respectively. The structures for all the possible orientation and adsorption sites were optimized using the density functional methodology with PBE1PBE/6-31G* level of theory. The PBE1PBE functional provides high in accuracy for weak and non-bonded interactions,[44] and is well suited for the present work, as is the 6-31G* basis function, commonly used for physisorption in carbon nanomaterials.[10,45,46] All the calculations were performed using Gaussian 09 (ref. 47) software. Frequency calculations were carried out on the fully optimized structures to confirm their minima. To calculate charge transfer, Mulliken charge[48] are used as they are available from orbital based *ab initio* calculations. However, these charges depend on the choice of basis set unlike Bader charges.[49] Nevertheless, recent studies[50,51] have shown that Mulliken charges are consistent with the Bader charge for charge transfer calculations, hence we report here charge transfer values based on Mulliken charges. The Total Density of States (TDOS) and the Partial Density of States (PDOS) plot were obtained using Multiwfn programs.[52]

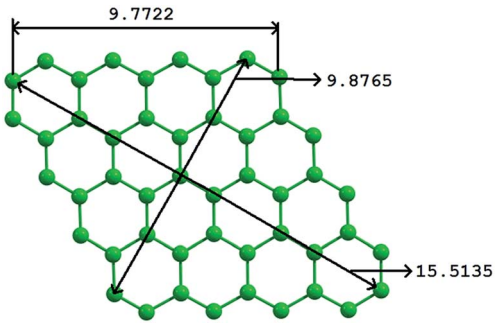

Fig. 1 Dimensions (Å) of graphene sheet considered.

The adsorption energy of CO_2 and H_2O on the graphene sheets was calculated using the formula:

$$E_{ad} = E_{(gas+graph)} - (E_{graph} + E_{gas})$$

where $E_{(gas+graph)}$, E_{graph} and E_{gas} are the total energies of the structure with the gas molecule adsorbed on graphene, bare graphene sheet and the isolated gas molecule respectively. Further, to study the effect of temperature on the hydrophobicity, the adsorption energy of H_2O on fluorine terminated sheets was calculated at four different temperatures, 323 K, 382 K, 441 K and 500 K respectively.

The electronic structure of the CO_2 and H_2O adsorbed complexes and the four kinds of graphene sheets are investigated, in order to obtain insight into the adsorption and sensing ability of the sheet for the gas molecules. The electronic structure is characterised by E_{HOMO} and E_{LUMO}, which represent the highest occupied molecular orbital (HOMO) energy and the lowest unoccupied molecular orbital (LUMO) energy, respectively. The difference between E_{LUMO} and E_{HOMO} is defined as the band gap, E_g, and

$$E_{L-H} = |E_{LUMO}(\text{Gr sheet}) - E_{HOMO}(\text{gas})|$$

$$E_{H-L} = |E_{LUMO}(\text{gas}) - E_{HOMO}(\text{Gr sheet})|$$

3. Results and discussion

3.1 Structure and energetics

The optimized geometries of the hydrogen and fluorine atoms terminated graphene sheets with and without the Stone–Thrower–Wales defect are shown in Fig. 5(a)–(d). The pristine sheet (sheet without defect) is also considered for comparison with the defect sheets. Table 1 provides the optimized structural parameters of the various sheets, showing the C–C bond lengths of the defect sheets to have a marginally wider range. The bond lengths on the zig-zag as well as the armchair edges also show a marginal but weaker increase. The smaller length of the C–C bonds of the armchair edges indicates them to be stronger than those on the zig-zag edges. Further, the C–H and C–F bonds in the hydrogen and fluorine terminated pristine graphene sheet (P-Gr/H,F) have bond length of 1.08 Å and 1.33 Å respectively. The Mulliken charge for all the hydrogen atoms along H-passivated edges have a uniform value of 0.173*e*. However,

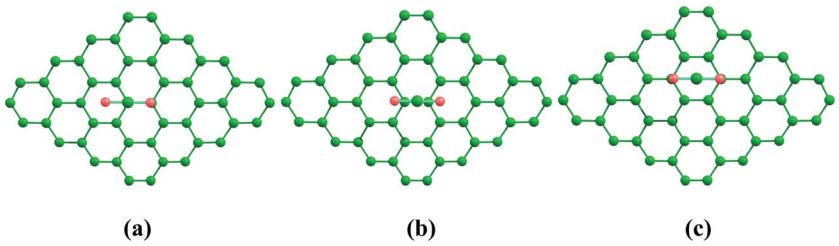

Fig. 2 Illustration of CO_2 adsorption on pristine graphene sheet in the parallel position, at a (a) top (T), (b) bridge (B), and (c) hollow (H) site.

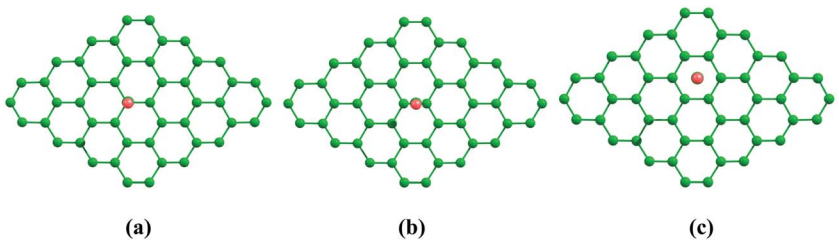

Fig. 3 Illustration of CO_2 adsorption on pristine graphene sheet in the perpendicular position, at a (a) top (T), (b) bridge (B), and (c) hollow (H) site.

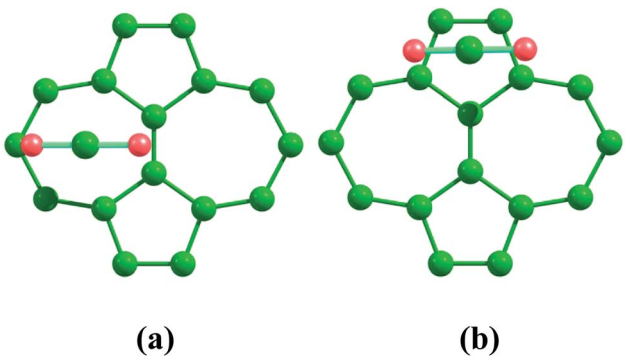

Fig. 4 Illustration of CO_2 adsorption at a Stone–Thrower–Wales defect in a graphene sheet, at a (a) hollow in heptagon (H-hept), and (b) hollow in pentagon (H-pent) site.

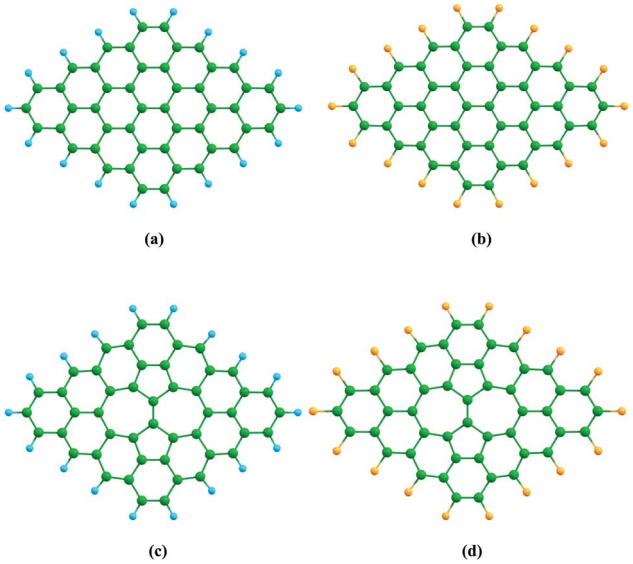

Fig. 5 Optimized structures of the four kinds of graphene sheets considered. (a) Hydrogen terminated pristine (P-Gr/H), (b) fluorine terminated pristine (P-Gr/F), (c) hydrogen terminated Stone–Thrower–Wales defected sheet (STW-Gr/H), and (d) fluorine terminated Stone–Thrower–Wales defected sheet (STW-Gr/F) sheet.

the fluorine atoms along the edges of the F-passivated sheet possess a charge value of $-0.257e$. This larger value for F is because of the electronegative nature of fluorine atoms, which results in electron density delocalization around the fluorine atoms, leaving the carbon atom positively charged, thereby making the C–F bond polar. The C–H and C–F bond length are unaltered due to the incorporation of Stone–Thrower–Wales defect. The C–C bond (vertical bond, rotated 90°) in the Stone–Thrower–Wales defect of the fluorine terminated sheets has a reduced bond length of 1.34 Å.

The formation energy of the STW defect in the F-terminated and H-terminated sheet is calculated using the formula:

$$E_F = E_{dg} - E_{pg}$$

where E_F is the defect formation energy, while E_{dg} and E_{pg} are the corresponding energies of the defect incorporated sheet and the pristine graphene sheet respectively. The above formula is appropriate when the number of carbon atoms in both the graphene and defect sheets is the same, as is the case here. Through this, we calculate the defect formation energy in hydrogen terminated sheet and fluorine terminated sheets to be, E_F(STW-Gr/H) = 3.1766 eV, and E_F(STW-Gr/F) = 3.3785 eV, respectively. This defect formation energy is the energy cost for the formation of the Stone–Thrower–Wales defect. It is evident that defect sheets having both kinds of terminations are equally feasible, based on their comparable formation energies.

Table 1 Optimized structural parameters of the four kinds of graphene sheets examined

Structures	Bond length (Å)	Zig-zag edge bond length (Å)	Armchair edge bond length (Å)
P-Gr/H	1.352–1.444	1.389–1.443	1.352–1.408
P-Gr/F	1.351–1.444	1.386–1.436	1.351–1.406
STW-Gr/H	1.347–1.471	1.385–1.451	1.363–1.408
STW-Gr/F	1.346–1.473	1.381–1.443	1.362–1.408

3.2 Adsorption of CO_2 and H_2O

In order to find the most favourable adsorption configurations, the gas molecules under investigation are initially placed above the graphene sheets. The gas molecules are placed with different orientations at different possible sites of adsorption on the graphene and with respect to the hexagon ring and the STW defect in the sheet. The adsorption height is determined by the minimum distance between the gas molecule and the graphene sheet normal to the surface.

3.2.1 CO_2. For the adsorption of CO_2, we take into account two possible orientations of CO_2. (i) The CO_2 molecule placed parallel to the graphene sheet (*i.e.* both carbon and oxygen adjacent to the sheet), and (ii) CO_2 placed perpendicular to the surface (*i.e.* the molecule axis is perpendicular to the graphene sheet with only one of the oxygen atoms adjacent to the sheet). Fig. 6 shows the optimized geometries of the most stable configurations of CO_2 adsorbed complexes. The various possible adsorption sites, bond length and bond angle of the adsorbed CO_2 molecule, adsorption energy and adsorption height and Mulliken charges of the molecule for the parallel orientation are listed in Table 2. Likewise, these parameters are listed in Table 3 for perpendicular orientation. The perpendicular orientation of CO_2 in the initial geometry optimizes to the parallel orientation of CO_2 with respect to the graphene surface, indicating that the CO_2 molecule prefers to align parallel to the graphene surface. Thus, in both initial orientations, the configuration of CO_2 converges to that corresponding to the same local energy minimum, *i.e.* CO_2 aligned parallel to the graphene plane and placed across the C–C bond of the graphene ring. Thus, the bridge position is the most stable site of adsorption on the examined graphene sheets for the CO_2 gas molecule. In particular, the CO_2 molecule prefers the bridge position of the pentagon ring on the STW-Gr/H sheet and the bridge position of the heptagon ring on the STW-Gr/F sheet.

In all the optimized configurations, the adsorption height (minimum atom to surface distance between the adsorbed CO_2 and the graphene sheet) varies from 3.42 Å to 3.47 Å. The most stable configurations of the adsorption of CO_2 on P-Gr/H, STW-Gr/H, P-Gr/F and STW-Gr/F sheets are identified by the letter 'a' in the 3rd column of Table 3. The adsorption energy of CO_2 on the most stable configurations of P-Gr/H, P-Gr/F, STW-Gr/H and STW-Gr/F sheets are −47.39 meV, −50.33 meV, −52.87 meV and −46.72 meV respectively, consistent with the physisorption energy for CO_2 of ∼50 meV on perfect graphene, reported by Liu *et al.*[53] The adsorption height of CO_2 on the STW-Gr/H is 3.45 Å,

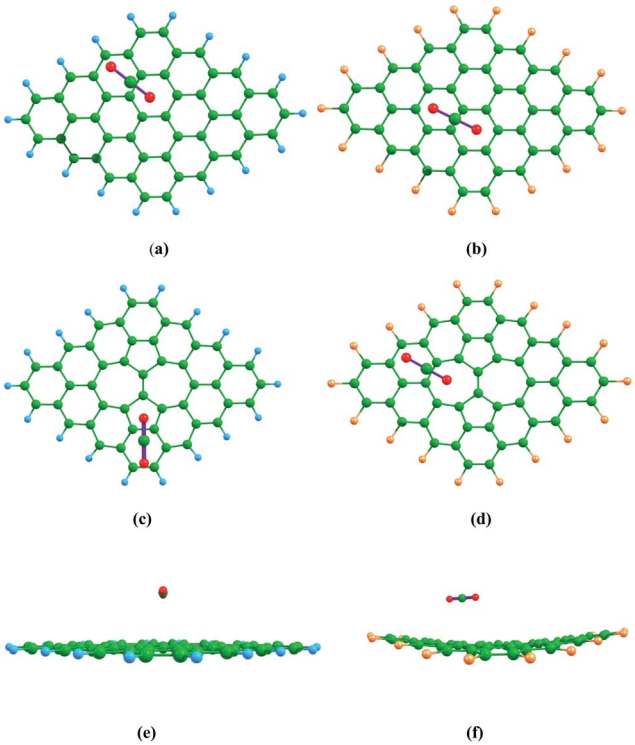

Fig. 6 Optimized geometries of stable configurations of CO_2 adsorbed complexes. (a) P-Gr/H with CO_2, (b) P-Gr/F sheet with CO_2, (c) STW-Gr/H sheet with CO_2, (d) STW-Gr/F sheet with CO_2. (e) and (f) are side views of (c) and (d) respectively.

which is 0.02 Å lower than on the pristine sheet. This lower adsorption height and the higher magnitude of the adsorption energy shows that the CO_2 molecules is more strongly physisorbed on the STW-Gr/H compared to the pristine sheet. The HOMO–LUMO band gap value of STW-Gr/H also increases to 1.43 eV from the value of 1.38 eV for the P-Gr/H sheet. Thus, the incorporation of the Stone–Thrower–Wales defect in the pristine hydrogen terminated sheet has significant influence on the adsorption of CO_2. In the case of fluorine terminated sheets, introducing the Stone–Thrower–Wales defect decreases the magnitude of the adsorption energy to 46.72 meV, despite the adsorption heights reducing to 3.42 Å (which is 0.04 Å lesser than the P-Gr/F). Thus, P-Gr/F (having adsorption energy of −50.33 meV) has better adsorption affinity for CO_2 than its defective counterpart STW-Gr/F. On introducing the Stone–Thrower–Wales defect in the F-terminated sheet, the graphene sheet suffers in-plane bending (Fig. 6f), due to the reduction of the electron density in the heptagon rings. The bond length of the CO_2 molecule in the adsorbed complex is unaltered from the free CO_2, while the bond angle is marginally reduced to 179.38° and 179.96° in the H- and F-terminated sheets respectively.

The charge transfer between the graphene sheet and the gas molecule using Mulliken population analysis provides a clear picture about the amount of donation or back donation of electrons between the systems. The negative values of Mulliken charges on the CO_2 indicate that the charges are transferred

Table 2 Structural parameters, adsorption energy, molecule height, and Mulliken charges for CO_2 molecule adsorbed in parallel position at different possible sites [top (T), hollow (H), bridge (B), H-hept (hollow at heptagon) and H-pent (hollow at pentagon)] on the four kinds of graphene sheet

Complex (adsorption of CO_2)	Adsorption sites-with parallel orientation		Total energy (Hartrees)	CO_2 bond length (Å), bond angle (deg.)	Adsorption energy E_{ad} (meV)	Molecule height d (Å)	Mulliken Charge (e)
	Initial	Final					
P-Gr/H	H	B	−2026.48115	1.165, 179.395	−43.58	3.44	−0.00271
	T	B	−2026.48109	1.165, 179.441	−41.94	3.44	−0.00233
	B	B	−2026.48117	1.165, 179.442	−44.13	3.47	−0.00239
P-Gr/F	H	B	−3811.00025	1.165, 179.935	−50.16	3.45	−0.00108
	T	B	−3811.00025	1.165, 179.961	−50.05	3.45	−0.00107
	B	B	−3811.00025	1.165, 179.961	−50.05	3.45	−0.00107
STW-Gr/H	H-hept	B	−2026.36433	1.165, 179.541	−41.44	3.47	−0.00263
	H-pent	B	−2026.36468	1.165, 179.259	−50.96	3.45	−0.00267
	T	B	−2026.36432	1.165, 179.554	−41.16	3.46	−0.00257
	B	B	−2026.36433	1.165, 179.541	−41.44	3.47	−0.00263
STW-Gr/F	H-hept	B	−3810.87587	1.165, 179.978	−44.07	3.42	−0.00203
	H-pent	B	−3810.87595	1.165, 179.837	−46.25	3.43	−0.00099
	T	B	−3810.87587	1.165, 179.978	−44.07	3.42	−0.00204
	B	B	−3810.87584	1.165, 179.933	−43.39	3.46	−0.00176

Table 3 Structural parameters, adsorption energy, molecule height, and Mulliken charges for CO_2 molecule adsorbed in perpendicular position at different possible sites [top (T), hollow (H), bridge (B), H-hept (hollow at heptagon) and H-pent (hollow at pentagon)] on the four kinds of graphene sheet

Complex (adsorption of CO_2)	Adsorption sites-with perpendicular orientation		Total energy (Hartrees)	CO_2 bond length (Å), bond angle (deg.)	Adsorption energy E_{ad} (meV)	Molecule height d (Å)	Mulliken charge (e)
	Initial	Final					
P-Gr/H	H	B	−2026.48123	1.165, 179.431	−45.75	3.46	−0.00235
	T	B[a]	−2026.48129	1.165, 179.386	−47.39	3.47	−0.00271
	B	B	−2026.48116	1.165, 179.364	−43.85	3.44	−0.00278
P-Gr/F	H	B	−3811.00025	1.165, 179.961	−50.32	3.46	−0.00107
	T	B[a]	−3811.00026	1.165, 179.961	−50.33	3.46	−0.00107
	B	B	−3811.00025	1.165, 179.941	−50.11	3.45	−0.00106
STW-Gr/H	H-hept	B	−2026.36466	1.165, 179.385	−50.42	3.44	−0.00291
	H-pent	B	−2026.36466	1.165, 179.385	−50.42	3.44	−0.00291
	T	B	−2026.36464	1.165, 179.402	−49.87	3.42	−0.00312
	B	B[a]	−2026.36475	1.165, 179.272	−52.87	3.45	−0.0021
STW-Gr/F	H-hept	B	−3810.87587	1.165, 179.978	−44.07	3.43	−0.00204
	H-pent	B	−3810.87595	1.165, 179.978	−46.47	3.43	−0.00099
	T	B[a]	−3810.87596	1.165, 179.978	−46.72	3.42	−0.0016
	B	B	−3810.87587	1.165, 179.978	−44.07	3.44	−0.00195

[a] Most stable configuration.

from the graphene sheet to the adsorbing gas molecules. From Table 3, it is seen that although the amount of charge transferred from the graphene sheet to CO_2 is larger in the hydrogen terminated than in the fluorine terminated sheet, the magnitude of adsorption energy is greater for the fluorine termination. This indicates that among the pristine sheets, fluorine termination is more favourable for CO_2 adsorption. Further, the hydrogen terminated sheet with the Stone–Thrower–Wales defect experiences similar charge transfer to the gas molecule as the pristine hydrogen terminated sheet, while the magnitude of the adsorption energy increases from 47.39 meV to 52.87 meV on introducing the defect. Thus, it is evident that the incorporation of the Stone–Thrower–Wales defect in the hydrogen terminated sheets increases the strength of adsorption of CO_2. On the contrary in the fluorine terminated sheet, pristine graphene has more affinity to CO_2 than the defect sheet, based on its higher magnitude of adsorption energy of 50.33 meV compared to 46.72 meV for STW-Gr/F. All the above results indicate that among the four sheets considered, STW-Gr/H has better adsorption affinity for CO_2 than the other sheets.

3.2.2 H_2O. Similar to CO_2, several initial adsorption configurations are considered for the adsorption of H_2O on graphene. The optimized geometries of the most stable configurations of H_2O on graphene are depicted in Fig. 7. The structural parameters of the adsorbed H_2O molecule on the graphene surface, along with its adsorption energy and adsorption height, for all the adsorbed complexes are given in Table 4. For discussion we have considered only the most stable configurations identified by the letter 'a' in the 3rd column of Table 4. For the adsorption of H_2O on the four kinds of graphene sheets, we find no significant changes in the structural parameters of the gas molecules (there is only a slight decrease in its bond angle and no change in bond length). This indicates that there is no substantiate charge transfer between the graphene sheet and the gas molecule, confirming that the interaction between the graphene sheet and the H_2O gas molecule is essentially that of physisorption. In the optimized geometries for the H_2O adsorbed systems, the position of H_2O varies from the initial position and it moves to the stable site of the adsorption (*i.e.* hollow site), unlike CO_2 which prefers the bridge site for adsorption. The adsorption height and energy for H_2O on the most stable configuration of hydrogen terminated pristine sheet are 2.81 Å and −101.25 meV respectively. Further, our adsorption energy value reasonably agrees with the energies reported by Courty[54] (−2.44 kcal mol^{-1}; −105.80 meV) and Sudiarta *et al.*[55] (−2.32 kcal mol^{-1}; −100.60 meV) based on their experimental and theoretical calculations respectively. Incorporation of the STW defect in the sheet of the most stable configurations, decreases the adsorption height to 2.79 Å, indicative of enhanced adsorption affinity for H_2O evident also from the higher magnitude of adsorption energy of −110.37 meV of the H_2O. The hydrogen atom of the H_2O molecule is closer to the graphene sheet for the P-Gr/H and STW-Gr/H compared to the F-terminated sheets, revealing the greater attractive nature of the carbon atoms of the H-terminated sheets towards the hydrogen atom of the water molecule *via* π–H interactions in the hydrogen terminated graphene sheet.

The fluorine terminated sheet shows some in-plane bending of the sheet on the introduction of the Stone–Thrower–Wales defect visible in Fig. 7f. In the optimized geometry, the oxygen atom of the H_2O is closer (atom to surface distance) to the fluorine terminated STW sheets as compared to the F-terminated pristine sheet. The reason may be due to the reduced electron density of the defect, which makes the carbon atoms of the sheet positive, thereby attracting the partial negative charge of the oxygen atom in the water molecule. The adsorption energy of the H_2O molecule on P-Gr/F and STW-Gr/F are −81.06 meV and −90.59 meV and its adsorption heights are 3.29 Å and 3.31 Å respectively. The adsorption height for H_2O is significantly increased in the fluorine terminated sheet compared to the hydrogen terminated sheet, from 2.79 Å to 3.31 Å for the STW sheet, and from 2.81 Å to 3.29 Å for the pristine sheet. This is a clear indication of increase of hydrophobicity on edge fluorination, evident also from the associated decrease in magnitude of the adsorption energy. Unlike CO_2 adsorption, STW-Gr/F has stronger adsorption for H_2O than the P-Gr/F, which is evident through the higher magnitude of the adsorption energy for the F-terminated STW sheet. The adsorption heights were measured from the oxygen atom of the water molecules to the graphene sheet, as the oxygen atom is closer to the graphene sheet. Thus, P-Gr/F and STW-Gr/F sheets have lower affinity energy for H_2O than hydrogen terminated sheets, and are more hydrophobic.

In all the systems, the negative values of Mulliken charges on the H_2O molecule indicate that the charge transfer from the graphene sheet to the water molecule is comparatively lower in STW-Gr/H (−0.00798*e*) than for the P-Gr/H (−0.01043*e*) sheet. On the contrary, the fluorine terminated sheets gain charge from the water molecule, in particular STW-Gr/F (0.00907*e*) gains more charge than P-Gr/F (0.008396*e*) from the water molecule due to the reduced electron density of the heptagon ring of the defect. Similar to the adsorption of CO_2, STW-Gr/H has better adsorption ability for H_2O than the other kinds of sheets examined, evident from its larger adsorption energy. In order to explore the effect of temperature on the hydrophobicity induced by the fluorination of graphene, we performed adsorption calculations for H_2O on both F-terminated sheets with and without STW defect at four different temperatures of 323 K, 382 K, 441 K and 500 K, and the results obtained are given in Table 5. From the adsorption energy values we see no significant influence of temperature on the adsorption of H_2O on STW-Gr/F, over the temperature range of 323–500 K; however in P-Gr/F, a minor decrease in the adsorption energy of H_2O, of the order of 6 meV, is observed at temperatures of 382 K and 441 K. These results indicate that the hydrophobic nature of fluorinated graphene sheets remains unchanged even beyond room temperature.

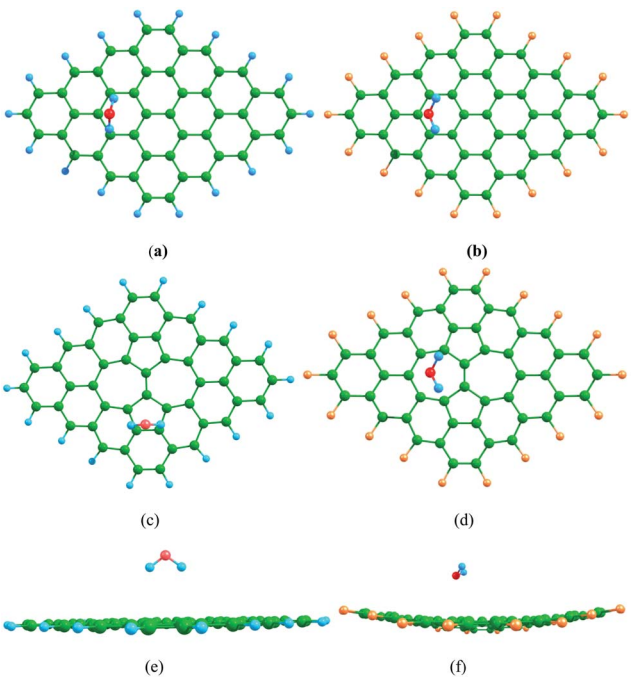

Fig. 7 Optimized geometries of stable configurations of H_2O adsorbed complexes. (a) P-Gr/H with H_2O, (b) P-Gr/F sheet with H_2O, (c) STW-Gr/H sheet with H_2O, (d) STW-Gr/F sheet with H_2O. (e) and (f) are side views of (c) and (d) respectively.

Table 4 Structural parameters, adsorption energy, molecule height, and Mulliken charges for H_2O molecule adsorbed at different possible sites [top (T), hollow (H), bridge (B), H-hept (hollow at heptagon) and H-pent (hollow at pentagon)] on four kinds of graphene sheet

Complex (adsorption of H_2O)	Adsorption sites		Total energy (Hartrees)	H_2O bond length (Å), bond angle (deg.)	Adsorption energy E_{ad} (meV)	Molecule height d (Å)	Mulliken charge (e)
	Initial	Final					
P-Gr/H	H	H	−1914.42629	0.965, 103.149	−100.44	2.77 (H)	−0.01074
	T	H[a]	−1914.42632	0.965, 103.137	−101.25	2.81 (H)	−0.01043
	B	H	−1914.42629	0.965, 103.188	−100.44	2.82 (H)	−0.00970
P-Gr/F	H	H	−3698.94442	0.965, 103.984	−80.54	3.34 (O)	0.007811
	T	H[a]	−3698.94444	0.965, 103.904	−81.06	3.29 (O)	0.008396
	B	H	−3698.94418	0.965, 103.984	−73.98	3.32 (O)	0.007887
STW-Gr/H	H-hept	H	−1914.30986	0.965, 103.269	−108.91	2.84 (H)	−0.01327
	H-pent	H[a]	−1914.30991	0.965, 103.037	−110.37	2.79 (H)	−0.007989
	T	H	−1914.30991	0.965, 103.037	−110.37	2.79 (H)	−0.007987
	B	H	−1914.30991	0.965, 103.036	−110.26	2.79 (H)	−0.00802
STW-Gr/F	H-hept	H[a]	−3698.82063	0.965, 104.006	−90.59	3.31 (O)	0.009071
	H-pent	H	−3698.82002	0.965, 103.898	−73.99	3.17 (O)	0.009452
	T	H	−3698.82002	0.965, 103.898	−74.05	3.17 (O)	0.009458
	B	H	−3698.82063	0.965, 104.006	−90.59	3.31 (O)	0.00907

[a] Most stable configuration.

Table 5 Effect of temperature on the hydrophobicity induced by fluorine-terminated graphene sheets

Temperature (K)	Adsorption energy of H_2O (meV)	
	P-Gr/F	STW-Gr/F
298	−81.06	−90.59
323	−81.01	−91.00
382	−74.80	−90.54
441	−74.80	−90.53
500	−80.99	−90.98

In summary, fluorine termination decreases affinity of graphene for the water molecule, and increases hydrophobicity for both pristine and STW sheets. Consistent with this increased hydrophobicity, the adsorption height increases for the fluorine terminated sheet compared to the hydrogen terminated sheet. Following the results in Table 4, fluorine termination reduces the magnitude of the adsorption energy of H_2O by about 20 meV for both the pristine and STW sheets, which corresponds to about 54% reduction in the Henry law constants, based on the Boltzmann factor. On the other hand, while it increases affinity for CO_2 on the pristine sheet, it reduces affinity for the STW sheet. Based on the increase in adsorption energy of about 3 meV on fluorine-termination of the pristine sheet, a 12% increase in the Henry law constant for CO_2 is predicted, while for the STW sheet the decrease in adsorption energy of about 5 meV corresponds to a reduction in the Henry law constant by 18%. The incorporation of the Stone–Thrower–Wales defect aids the adsorption of both H_2O and CO_2 in the sheet, except for the STW-Gr/F sheet in which the adsorption ability for CO_2 decreases. While these studies have been performed with graphene sheets of small dimension (4×4 rhombic sheet of side ~9.77 Å), it would be interesting to study the effect of sheet size on both kinds of functionalization. Based on earlier studies[55,56] we speculate here that the functionalization will have negligible effect with respect to increase in the sheet size beyond a certain value. It therefore remains to investigate the range of sheet sizes over which the functionalised edge sites will have significant influence. This trend will be explored in subsequent work. Further insights of the adsorption are obtained from the electronic properties of the graphene sheets, discussed below.

3.3 Electronic properties

3.3.1 HOMO–LUMO gap. The HOMO–LUMO distributions (depicted in Fig. S1 of the ESI†) indicate that the hydrogen terminated sheets have delocalization of the π-electron cloud over the carbon atoms, while the hydrogen atoms do not have any charge population. However, in the case of fluorine terminated sheets, both the HOMO and LUMO have charges of sigma orbitals localized on the fluorine atoms, while the π-electron cloud are on the carbon atoms. In the defect sheet involving hydrogen and fluorine termination, the heptagon ring of the defect possess little amount of π-electron cloud, whereas sigma orbital of electrons are localized on the rotated C–C bond of the Stone–Thrower–Wales defect. The 90° rotation of the C–C bond has very little influence on the electron density, evident from the HOMO and LUMO plot.

From the HOMO–LUMO distribution for the most stable configurations of CO_2 adsorbed complexes (depicted in Fig. S2†), it is evident that the carbon dioxide molecule does not lead to any changes in the HOMO as well as LUMO orbital distributions, indicative of the physisorptive nature of the interaction. The frontier orbital energy difference of the graphene sheet and the gas molecules and the band gap values for the adsorbed systems are listed in Table 6. The energy gap value of the defect sheet is 0.05 eV higher than the pristine sheet for both hydrogen and fluorine termination. The HOMO–LUMO gaps of the four kinds of graphene sheet show no appreciable change on the adsorption of CO_2 and H_2O. From the table, it is

Table 6 Band gap for the bare sheet, and E_{L-H}, E_{H-L} for the adsorption of CO_2 and H_2O on four kinds of graphene sheet

Complex	Band gap of bare sheet (eV)	Adsorption of CO_2			Adsorption of H_2O		
		Band gap (eV)	E_{L-H} (eV)	E_{H-L} (eV)	Band gap (eV)	E_{L-H} (eV)	E_{H-L} (eV)
P-Gr/H	1.379	1.379	7.445	5.535	1.381	5.316	6.577
P-Gr/F	1.349	1.349	6.685	6.264	1.349	4.557	7.306
STW-Gr/H	1.429	1.431	7.566	5.462	1.432	5.438	6.505
STW-Gr/F	1.401	1.403	6.803	6.198	1.404	4.675	7.241

noted that for all the four types of graphene sheet considered, the frontier orbital energy difference for the adsorption of CO_2 follow $E_{L-H} > E_{H-L}$. The energy difference between E_{L-H} and E_{H-L} is higher for the hydrogen terminated sheet than for the fluorine terminated sheet. Thus, in the P-Gr/H sheet an electron has to overcome a barrier of 5.535 eV for transfer to the gas molecule, whereas the gas molecule needs to cross the barrier of 7.445 eV to transfer an electron to the P-Gr/H. Consequently, the P-Gr/H prefers to transfer the electrons to the CO_2 molecule. The large difference in the value of $E_{L-H} - E_{H-L}$, also accounts for larger charge transfer from the hydrogen terminated sheet to the CO_2 molecule compared to the F-terminated sheet. In the case of fluorine terminated sheets, the energy difference between E_{L-H} and E_{H-L} is much smaller compared to the hydrogen terminated sheets, due to the presence of electronegative fluorine atoms in the sheet. Hence, the charges transferred from the graphene sheet to CO_2 in P-Gr/F and STW-Gr/F are comparably lower than in the P-Gr/H and STW-Gr/H sheets.

The HOMO and LUMO distribution of the stable configurations of H_2O adsorbed complexes (*cf.* Fig. S3 of ESI†) do not vary significantly from the bare graphene sheet, due to the physisorptive nature of the interaction and there is no localization of electrons around the water molecule. The frontier molecular orbital energy difference between the water molecule and the graphene sheet follows $E_{H-L} > E_{L-H}$ for all the four kinds of sheets, so that H_2O provides electrons to the graphene surface. The energy difference between E_{H-L} and E_{L-H} is higher for the fluorine terminated sheets than for the hydrogen terminated sheets, opposite to the case of CO_2 adsorption. The reason for this behaviour may be due to the localization of electron density along the edges of fluorine terminated sheets, evident through its HOMO–LUMO plot in Fig. S3.† In the P-Gr/F and STW-Gr/F graphene sheets the electrons require an energy in excess of 7.306 eV and 7.241 eV respectively, for their transfer to the water molecule. However, for charge transfer from water to the sheet the corresponding energy required for electron is lesser that is 4.557 eV and 4.675 eV. Therefore, the sheets gain charges from the adsorbed water molecule. The corresponding Mulliken charges of H_2O on the adsorbed complexes of P-Gr/F and STW-Gr/F are 0.008396*e* and 0.00907*e* respectively. On the whole, from the above results it is seen that more facile charge transfer occurs in the adsorption of water molecules on the fluorine terminated sheets compared to the H-terminated sheets.

3.3.2 Density of states. To understand the electronic structure of the physisorbed complex, the Total Density of

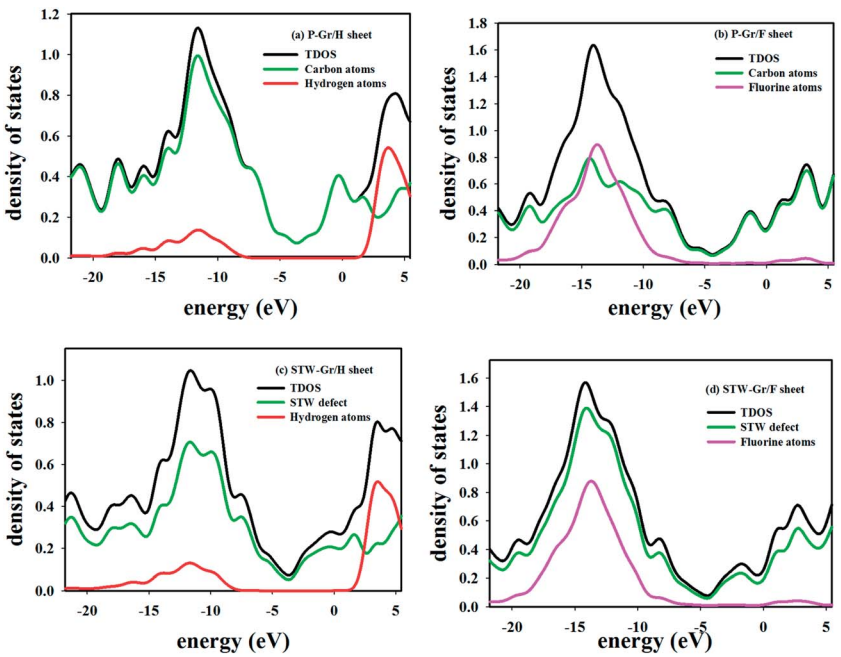

Fig. 8 TDOS and PDOS of four kinds of sheets considered, in the absence of adsorption.

Table 7 Fermi level for the bare sheet, for the adsorption of CO_2 and H_2O on four kinds of graphene sheet

	Fermi level (eV)		
Graphene sheet	Bare sheet	CO_2	H_2O
P-Gr/H	−3.66	−3.67	−3.76
P-Gr/F	−4.41	−4.41	−4.33
STW-Gr/H	−3.56	−3.58	−3.64
STW-Gr/F	−4.31	−4.32	−4.25

States (TDOS) and the Partial Density of States (PDOS) are calculated for the CO_2 and H_2O adsorbed complexes, along with the bare graphene sheets. The TDOS and PDOS plots for the bare graphene sheets are depicted in Fig. 8(a)–(d), and the Fermi levels of the bare graphene sheets and the adsorbed complexes are listed in Table 7. In the PDOS of P-Gr/H, the hydrogen atoms terminated at the edges provide meagre contribution to HOMO and the high-lying regions of LUMO. The peaks of carbon atoms do not change significantly from the TDOS for both the H and F functionalised sheets, indicating that the edge functionalisation does not influence the electronic structure of the graphene sheet. Initially the Fermi level of the P-Gr/H is located at −3.66 eV and the inclusion of Stone–Thrower–Wales defect leads to the broadening of the valence bands, which subsequently shifts the Fermi level to −3.56 eV. The distinct double peak in the TDOS of STW-Gr/H appears due to the 90° rotation of the C–C bond in the Stone–Thrower–Wales defect, which is also visible in the PDOS. The contribution of hydrogen atoms and the Fermi level position remains the same in both the defect and pristine form.

In the case of the fluorine-terminated sheet, Fig. 8 indicates that the fluorine atoms have their peaks in the valence band region alone, with no contribution to the conduction bands. Further, as fluorine atoms act as acceptors, the Fermi level downshifts to the valence band at −4.41 eV. Thus, the contribution of fluorine atoms in the valence band region is significant. Likewise, in the PDOS of STW-Gr/F the Fermi level also shifts towards the valence bands at −4.31 eV. Thus, fluorine termination downshifts the Fermi level by upto 0.7 eV compared to hydrogen termination. In the defect sheet, even though the fluorine atoms have significant contribution in HOMO, the contribution of the Stone–Thrower–Wales defect is higher, which is visible through the peaks. Thus, the Stone–Thrower–Wales defect in the fluorine terminated sheets is responsible for the peak height reduction of TDOS in the valence band region.

The TDOS and PDOS for the adsorption of CO_2 on the four kinds of graphene sheets are shown in Fig. 9. From the figures, we observed that there is no significant change in the Fermi level compared with the bare sheet, indicating that the electronic structure of the sheet does not change after adsorption. The curves shows only minor changes on adsorbing CO_2, confirming the weak interaction. The total density of states for the CO_2-adsorbed systems is localized between −16.6 eV and −8.6 eV and around 0.18 eV and 4.4 eV (values are from Fig. 9) in the valence and conduction bands respectively. This suggest that adsorption of molecule CO_2 has made significant changes in the low-lying valence and the conduction bands. Likewise, the adsorption of CO_2 on P-Gr/H and STW-Gr/H has induced some prominent peaks in the HOMO. The peak height of the HOMO is pronounced in the P-Gr/F and STW-Gr/F sheets, indicating that the CO_2 adsorption has influenced the valence band region.

The TDOS and PDOS plots for the adsorption of H_2O on the four kinds of graphene sheets are depicted in Fig. 10. The

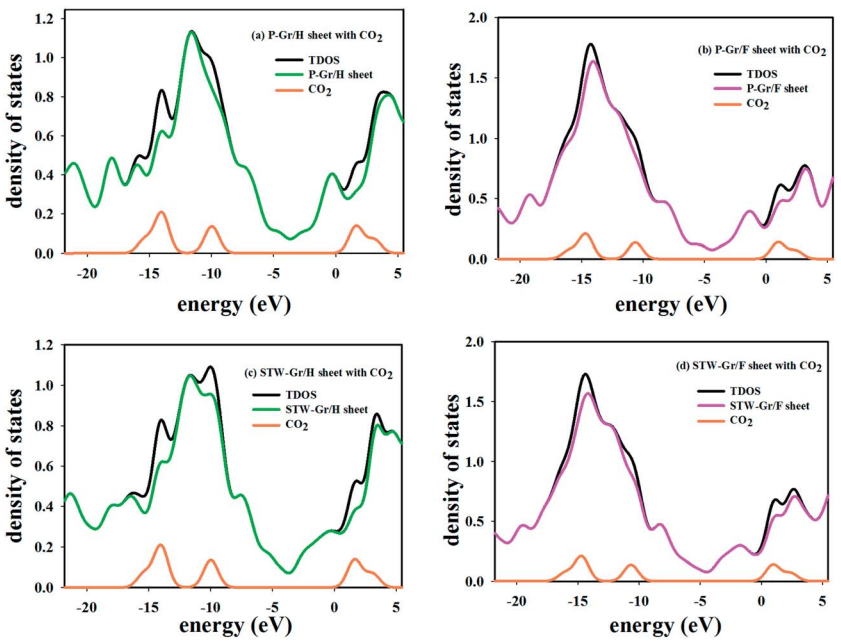

Fig. 9 TDOS and PDOS of H_2O adsorbed complexes for the four kinds of sheets considered.

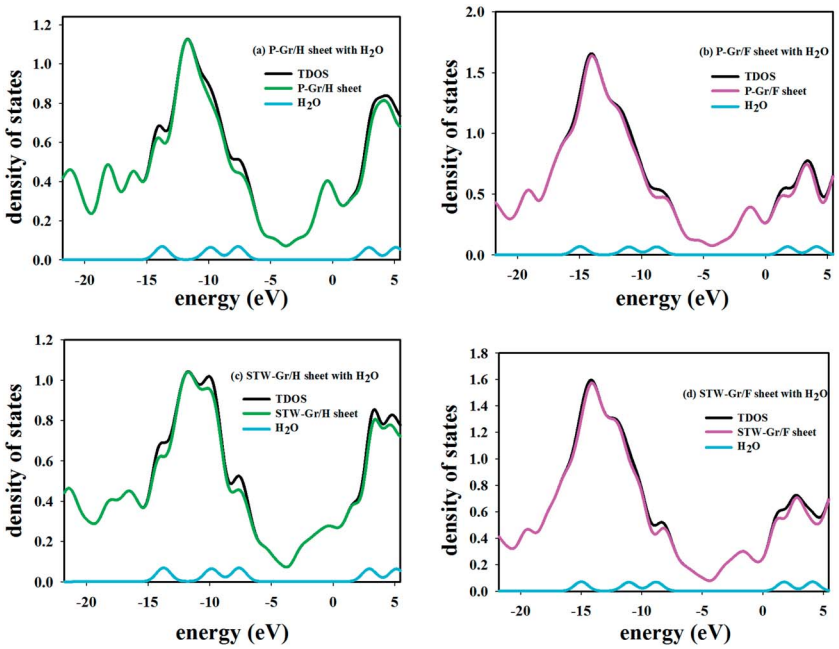

Fig. 10 TDOS and PDOS of H_2O adsorbed complexes for the four kinds of sheets considered.

adsorption of H_2O on both hydrogen and fluorine terminated sheets, does not have any impact on the Fermi-level, evident through Table 7. This behaviour reveals that the electronic structure of the fluorinated sheet is not changed due to the adsorption of H_2O. After the adsorption of H_2O, the density of states does not change drastically, indicating the weak interaction. Indeed, the changes in the density of states are smaller for the adsorption of H_2O compared to CO_2. Among the four sheets, STW-Gr/H does show a minor change due to the adsorption of H_2O. The total DOS for the adsorbed systems is localized between −15.38 eV and −6.44 eV in the valence bands and around 1.66 eV in the conduction bands.

Thus, the graphene sheet is not significantly influenced in its valence and conduction bands due to hydrogen termination, whereas there is a substantial effect on its valence bands due to fluorine termination, evident through the increase in peak heights. The changes in the total density of states on adsorption of CO_2 is more significant than the adsorption of H_2O.

4. Conclusion

The co-adsorption of H_2O, which saturates industrial and power plant flue gas emissions, has been a major impediment to the development of processes for CO_2 capture. Our results show that edge fluorination of pristine graphene offers an attractive route for enhancing hydrophobicity, while increasing affinity for CO_2, thereby inhibiting H_2O co-adsorption. We find that for pristine graphene sheets, hydrogen termination leads to stronger adsorption of H_2O than fluorine termination, while the opposite is the case for CO_2. On the other hand, incorporation of Stone–Thrower–Wales defects enhances adsorption of both CO_2 and H_2O molecules compared to the pristine sheet, and in these sheets hydrogen termination leads to stronger adsorption for both gas molecules as compared to fluorine termination. While our investigations have centred around graphene, these results are expected to hold in general for nanoporous carbons, due to their underlying turbostractic structure comprising defective and misaligned graphene sheets. Such carbons are increasingly being considered as an attractive alternative for CO_2 capture, due to their intrinsic hydrophobicity when free from hydrophilic surface functionalities.[39] All the above findings imply that the pristine graphene sheets and carbons with fluorine passivation of edge sites, and having high degree of short-range ordering, are good candidates for CO_2 adsorption while suppressing co-adsorption of H_2O.

Acknowledgements

One of the authors (LS) thanks the Indian National Science Academy (INSA) for providing support through the Indo-Australia Early Career Visiting Fellowship, enabling his stay at the University of Queensland during July 2013–June 2014.

References

1 A. K. Geim and K. S. Novoselov, *Nat. Mater.*, 2007, **6**, 183–191.
2 E. Yoo, J. Kim, E. Hosono, H.-s. Zhou, T. Kudo and I. Honma, *Nano Lett.*, 2008, **8**, 2277–2282.
3 K. S. Novoselov, A. K. Geim, S. V. Morozov, D. Jiang, Y. Zhang, S. V. Dubonos, I. V. Grigorieva and A. A. Firsov, *Science*, 2004, **306**, 666–669.
4 N. Mohanty and V. Berry, *Nano Lett.*, 2008, **8**, 4469–4476.
5 D.-e. Jiang, V. R. Cooper and S. Dai, *Nano Lett.*, 2009, **9**, 4019–4024.
6 T. Wu, Q. Xue, C. Ling, M. Shan, Z. Liu, Y. Tao and X. Li, *J. Phys. Chem. C*, 2014, **118**, 7369–7376.

7 K. Brenner, Y. Yang and R. Murali, *Carbon*, 2012, **50**, 637–645.
8 P. A. Thrower, *Chemistry and Physics of Carbon*, ed. P. L. Walker, Dekker, New York, 1969, vol. 5, p. 262.
9 A. J. Stone and D. J. Wales, *Chem. Phys. Lett.*, 1986, **128**, 501–503.
10 H. Tachikawa and T. Iyama, *Solid State Sci.*, 2014, **28**, 41–46.
11 M. Pagliaro and R. Ciriminna, *J. Mater. Chem.*, 2005, **15**, 4981–4991.
12 A. Mathkar, T. N. Narayanan, L. B. Alemany, P. Cox, P. Nguyen, G. Gao, P. Chang, R. Romero-Aburto, S. A. Mani and P. M. Ajayan, *Part. Part. Syst. Charact.*, 2013, **30**, 266–272.
13 W. Dai, S. J. Kim, W. K. Seong, S. H. Kim, K. R. Lee, H. Y. Kim and M. W. Moon, *Sci. Rep.*, 2013, **3**, 2524.
14 K. Celebi, J. Buchheim, R. M. Wyss, A. Droudian, P. Gasser, I. Shorubalko, J.-I. Kye, C. Lee and H. G. Park, *Science*, 2014, **344**, 289–292.
15 R. B. Dos Santos, R. Rivelino, F. D. B. Mota and G. K. Gueorguieve, *J. Phys. Chem. A*, 2012, **116**, 9080–9087.
16 C. Sun, M. S. H. Boutilier, H. Au, P. Poesio, B. Bai, R. Karnik and N. G. Hadjiconstantinou, *Langmuir*, 2013, **30**, 675–682.
17 H. Li, Z. Song, X. Zhang, Y. Huang, S. Li, Y. Mao, H. J. Ploehn, Y. Bao and M. Yu, *Science*, 2013, **342**, 95–98.
18 H. W. Kim, H. W. Yoon, S.-M. Yoon, B. M. Yoo, B. K. Ahn, Y. H. Cho, H. J. Shin, H. Yang, U. Paik, S. Kwon, J.-Y. Choi and H. B. Park, *Science*, 2013, **342**, 91–95.
19 T. Yumura and A. Yamasaki, *Phys. Chem. Chem. Phys.*, 2014, **16**, 9656–9666.
20 L. Liu and S. K. Bhatia, *J. Phys. Chem. C*, 2013, **117**, 13479–13491.
21 T. X. Nguyen and S. K. Bhatia, *J. Phys. Chem. C*, 2011, **115**, 16606–16612.
22 T. X. Nguyen and S. K. Bhatia, *J. Phys. Chem. C*, 2012, **116**, 3667–3676.
23 M. H. Gass, U. Bangert, A. L. Bleloch, P. Wang, R. R. Nair and A. K. Geim, *Nat. Nanotechnol.*, 2008, **3**, 676–681.
24 Y. H. Zhang, Y.-B. Chen, K.-G. Zhou, C.-H. Liu, J. Zeng, H.-L. Zhang and Y. Peng, *Nanotechnology*, 2009, **20**, 185504.
25 G. K. Gueorguieve, A. Furlan, H. Hogberg, S. Stafstrom and L. Hultman, *Chem. Phys. Lett.*, 2006, **426**, 374–379.
26 J. Ma, D. Alfè, A. Michaelides and E. Wang, *Phys. Rev. B: Condens. Matter Mater. Phys.*, 2009, **80**, 033407.
27 F. Banhart, J. Kotakoski and A. V. Krasheninnikov, *ACS Nano*, 2010, **5**, 26–41.
28 V. H. Crespi, M. L. Cohen and A. Rubio, *Phys. Rev. Lett.*, 1997, **79**, 2093–2096.
29 F. Banhart, *Rep. Prog. Phys.*, 1999, **62**, 1181.
30 B. W. Smith and D. E. Luzzi, *J. Appl. Phys.*, 2001, **90**, 3509–3515.
31 A. Hashimoto, K. Suenaga, A. Gloter, K. Urita and S. Iijima, *Nature*, 2004, **430**, 870–873.
32 R. Song, S. Wangmo, M. Xin, Y. Meng, P. Huai, Z. Wang and R. Zhang, *Nanoscale*, 2013, **5**, 6767–6772.
33 D. Dutta, B. C. Wood, S. Y. Bhide, K. G. Ayappa and S. Narasimhan, *J. Phys. Chem. C*, 2014, **118**, 7741–7750.
34 X. Qin, Q. Meng and W. Zhao, *Surf. Sci.*, 2011, **605**, 930–933.
35 Q. M. X. Qin and W. Zhao, *International Conference in Nanotechnology and Biosensors*, IACSIT Press, 2011, pp. 80–84.
36 N. Ghaderi and M. Peressi, *J. Phys. Chem. C*, 2010, **114**, 21625–21630.
37 Y.-H. Zhang, L.-F. Han, Y.-H. Xiao, D.-Z. Jia, Z.-H. Guo and F. Li, *Comput. Mater. Sci.*, 2013, **69**, 222–228.
38 H. Liu, S. Dai and D.-e. Jiang, *Nanoscale*, 2013, **5**, 9984–9987.
39 S. K. Bhatia and T. X. Nguyen, *Ind. Eng. Chem. Res.*, 2011, **50**, 10380–10383.
40 Y. Liu and J. Wilcox, *Environ. Sci. Technol.*, 2012, **46**, 1940–1947.
41 Y. Wang and M. D. LeVan, *J. Chem. Eng. Data*, 2009, **54**, 2839–2844.
42 J. Liu, Y. Wang, A. I. Benin, P. Jakubczak, R. R. Willis and M. D. LeVan, *Langmuir*, 2010, **26**, 14301–14307.
43 P. A. Webley, *Adsorption*, 2014, **20**, 225–231.
44 Y. Zhao and D. G. Truhlar, *J. Chem. Theory Comput.*, 2005, **1**, 415–432.
45 D. Umadevi and G. N. Sastry, *J. Phys. Chem. Lett.*, 2011, **2**, 1572–1576.
46 D. Umadevi and G. N. Sastry, *Curr. Sci.*, 2014, **106**, 1224–1234.
47 M. J. Frisch, G. W. Trucks, H. B. Schlegel, G. E. Scuseria, M. A. Robb, J. R. Cheeseman, G. Scalmani, V. Barone, B. Mennucci, G. A. Petersson, H. Nakatsuji, M. Caricato, X. Li, H. P. Hratchian, A. F. Izmaylov, J. Bloino, G. Zheng, J. L. Sonnenberg, M. Hada, M. Ehara, K. Toyota, R. Fukuda, J. Hasegawa, M. Ishida, T. Nakajima, Y. Honda, O. Kitao, H. Nakai, T. Vreven, J. A. Montgomery, J. E. Peralta, F. Ogliaro, M. Bearpark, J. J. Heyd, E. Brothers, K. N. Kudin, V. N. Staroverov, R. Kobayashi, J. Normand, K. Raghavachari, A. Rendell, J. C. Burant, S. S. Iyengar, J. Tomasi, M. Cossi, N. Rega, J. M. Millam, M. Klene, J. E. Knox, J. B. Cross, V. Bakken, C. Adamo, J. Jaramillo, R. Gomperts, R. E. Stratmann, O. Yazyev, A. J. Austin, R. Cammi, C. Pomelli, J. W. Ochterski, R. L. Martin, K. Morokuma, V. G. Zakrzewski, G. A. Voth, P. Salvador, J. J. Dannenberg, S. Dapprich, A. D. Daniels, O. Farkas, J. B. Foresman, J. V. Ortiz, J. Cioslowski and D. J. Fox, in *Gaussian 09, Revision B.01*, Gaussian, Inc., Wallingford CT, 2009.
48 R. S. Mulliken, *J. Chem. Phys.*, 1955, **23**, 1833.
49 R. F. W. Bader, *Chem. Rev.*, 1991, **91**, 893–928.
50 J. Wang, W. Luo, J. Feng, L. Zhang, Z. Li and Z. Zou, *Phys. Chem. Chem. Phys.*, 2013, **15**, 16054–16064.
51 C. G. Da Rocha, P. A. Clayborne, P. Koskinen and H. Hakkinen, *Phys. Chem. Chem. Phys.*, 2014, **16**, 3558–3565.
52 T. Lu, *Multiwfn 2.1*, http://multiwfn.codeplex.com/.
53 Y. Liu and J. Wilcox, *Environ. Sci. Technol.*, 2010, **45**, 809–814.
54 A. Courty, *et al.*, *J. Phys. Chem. A*, 1998, **102**, 6590–6600.
55 I. Wayan Sudiarta and D. J. Wallance Geldart, *J. Phys. Chem. A*, 2006, **110**, 10501–10506.
56 D. B. Karki and N. P. Adhikari, arXiv preprint arXiv:1404.6446, 2014.